DOI: 10.19884/j.1672-5220.202510006

Nanofiber/Zwitterionic Hydrogel Composite for Anti-Foreign Body Reaction

DANG Xiangyu, GAO Yujie, CHEN Zhize *
Key Laboratory of Sustainable Low-carbon Technologies for Textile Dyeing and Finishing, Ministry of Education, College of Chemistry and Chemical Engineering, Donghua University, Shanghai 201620, China

Abstract: In this study, we developed a nanofiber/zwitterionic hydrogel composite aimed at overcoming the in vivo foreign body reaction. This composite leverages the adhesive properties of polydopamine (PDA) to integrate trimethylamine *N*-oxide (TMAO) zwitterionic hydrogel with a three-dimensional poly(lactic acid) (PLA) nanofiber membrane. The resulting material exhibits the robust mechanical properties characteristic of PLA, featuring a tensile strength of approximately 13 MPa and an elongation at break exceeding 20%. Furthermore, owing to the TMAO zwitterionic hydrogel, the composite demonstrates exceptional resistance to biological contamination. After 30 d in a murine model, the composite does not develop a dense collagen layer on its surface, maintaining a thickness of less than 30 μm.

Keywords: nanofiber; hydrogel; anti-foreign body reaction; zwitterion
CLC number: R392.4 **Document code**: A
Article ID: 1672-5220(2026)03-0032-12

Open Science Identity (OSID)

0 Introduction

Biomaterials derived from synthetic and natural polymers are crucial in medical applications, including regenerative medicine, drug delivery, and implants. Their use has accelerated advancements in biomedicine and significantly enhanced human quality of life[1-2]. However, any material introduced into a living organism elicits a response from the immune system, termed a foreign body reaction[3]. While the foreign body reaction at the implant surface can shield the organism from bacteria, viruses, and physical damage, it may also result in the encapsulation of the implant, thereby impairing its functionality. Consequently, the implant may require removal or replacement through a secondary surgical procedure, which increases costs and elevates the risks of injury or mortality[4]. The foreign body reaction is typically characterized by four stages: protein adsorption, acute inflammation, chronic inflammation, and collagen coating[5-6]. The process begins with non-specific protein adsorption. Consequently, strategies aimed at preventing protein adsorption present a promising approach for mitigating the foreign body reaction.

Electrospun nanofibers, bearing a striking resemblance in structure and mechanical characteristics to the extracellular matrix (ECM), have garnered significant interest in the realms of tissue regeneration and drug delivery[7-9]. However, the exceptionally high specific surface area of nanofibers results in significant non-specific protein adsorption, which subsequently induces the foreign body reaction[10-12]. Studies have demonstrated that enhancing surface hydrophilicity can markedly decrease protein adsorption, reduce the adhesion of inflammatory cells, and mitigate unnecessary immune responses[12-14]. Polyethyleneglycol (PEG) and polyhydroxyethyl methacrylate (PHEMA) are commonly utilized in implant materials. Both polymers are rich in hydroxyl groups, which contribute to their favorable hydrophilicity. Nevertheless, these materials can still elicit a foreign body reaction following implantation[15-16]. Zwitterionic polymers are extensively utilized in materials designed to prevent biological contamination, owing to their pronounced hydrophilicity. Each repeating unit of these polymers contains equal quantities of positive and negative charges. In contrast to PEG and PHEMA, zwitterionic hydrogels can create a hydration shell on material surfaces via electrostatic interactions and serve as physical barriers to inhibit protein adhesion[17]. Zhang et al.[18] showed that the poly(carboxybetaine methacrylate) (PCB) hydrogel exhibited notable resistance to the foreign body reaction in mice at three months post-subcutaneous implantation. Despite their excellent biocompatibility and robust resistance to biological contamination, the biological applications of zwitterionic hydrogels remain constrained by their inadequate mechanical strength[19]. Composites that integrate hydrogels with electrospun nanofibers have garnered significant interest from researchers, owing to their favorable structural compatibility and biological functions[20]. Nanofiber/hydrogel composites combine the biocompatibility of hydrogels with the superior mechanical properties of nanofibers. In recent years,

Received date: 2025-10-19
Foundation item: Fundamental Research Funds for the Central Universities, China (No. 2232025A-09)
* Correspondence should be addressed to CHEN Zhize, email: chenzhize@dhu.edu.cn
Citation: Dang X Y, Gao Y J, Chen Z Z. Nanofiber/zwitterionic hydrogel composite for anti-foreign body reaction[J]. *Journal of Donghua University (English Edition)*, 2026, 43(3): 32-43.

these composites have advanced significantly in biomedical applications, including regenerative medicine, tissue engineering, and drug delivery[21].

In this study, we employed poly (lactic acid) (PLA) electrospun nanofiber membranes as the "mechanical skeleton" of the composite system, which provided stable structural support for the hydrogel and improved the overall mechanical properties of the composite. PLA is a well-recognized bio-based polyester material. Its degradation product is lactic acid, which can be eliminated via the human metabolic pathway without inducing local inflammatory responses or toxic accumulation[22]. The electrospinning technique enables the fabrication of nanofiber membranes with a high specific surface area and interconnected porous structure. This architecture not only serves as a stable three-dimensional scaffold for hydrogel loading, but also mimics the native ECM. Concurrently, trimethylamine *N*-oxide (TMAO) zwitterionic hydrogel served as the functional coating. TMAO is an intestinal microbial metabolite derived from dietary choline and carnitine. The positive and negative charges of TMAO are intrinsically linked, and its interaction with water is notably stronger, leading to an increased water density within the hydrated layer. Consequently, TMAO is considered a highly promising antifouling material. The TMAO hydrogel coating significantly enhances the hydrophilicity and biocompatibility of PLA nanofiber membranes, while also markedly reducing the foreign body reaction. Furthermore, the composite structure created by the two components can accommodate both porosity and high permeability, facilitating efficient material exchange between the interior and exterior of the material and establishing an appropriate physiological microenvironment for the implantation site. Two TMAO zwitterionic hydrogels were synthesized with different feeding ratios of TMAO monomers to —COOH groups on poly(itaconic acid) (PIA) chains (50% and 70%, respectively). The resulting hydrogels were designated as $PIAPMANO_{50}$ and $PIAPMANO_{70}$, where the numbers 50 and 70 in the sample codes represent these feeding molar ratios in percent. Different molar ratios of *N*, *N*-dimethyl-3-aminopropylamine *N*-oxide (DMAPANO) and *N*-(3-aminopropyl) methacrylamide hydrochloride (APMA) were introduced into PIA via amidation reaction to fabricate the hydrogel precursor. Subsequent ultraviolet (UV)-initiated cross-linking constructed a three-dimensional network structure. To resolve the interfacial compatibility challenge between hydrophilic hydrogels and hydrophobic PLA nanofiber membranes, we employed the self-polymerization of dopamine (DA) into polydopamine (PDA) under alkaline conditions. The hydroxyl groups and benzene rings in PDA can form hydrogen bond interactions and π-π stacking interactions with the ester groups in the PLA molecules. Meanwhile, the abundant hydroxyl and amino groups in PDA can form a dense hydrogen bond network with the hydrogel. This process resulted in the formation of a film on the surface of the PLA nanofiber membrane, characterized by active catechol and amino groups. This modification not only enhanced hydrophilicity but also improved adhesion, thereby increasing the durability of the hydrogel coating. To assess the anti-foreign body reaction capability of the composite, we concurrently implanted the composite and PEG hydrogel into the abdominal cavity of mice.

1 Materials and Methods

1.1 Materials

Itaconic acid (IA), ammonium persulfate (APS), *N*,*N*-dimethyl-1,3-propane diamine (DMAPA), 4-(4,6-dimethoxy-1,3,5-triazin-2-yl)-4-methylmorpholinium chloride (DMTMM), APMA, hexafluoroisopropanol (HFIP), 2-hydroxy-2-methylpropiophenone (photoinitiator 1173), poly(ethylene glycol) diacrylate (PEGDA, number-average molecular mass M_n of 2×10^6) were obtained from Shanghai Aladdin Biochemical Technology Co., China. Hydrogen peroxide (H_2O_2, mass fraction of 30%), acetone, ethanol, ether, methanol, dimethyl sulfoxide (DMSO), *N*,*N*-dimethylformamide (DMF), deuterated water, phosphate buffered saline (PBS) buffer (0.01 mol/L, pH 7.2), and sterile saline were obtained from Sinopharm Chemical Reagent Co., Ltd., China. Fluorescently labeled bovine serum albumin (FITC-BSA) was obtained from Beijing Solepol Technology Co., Ltd., China. Trihydroxymethylaminomethane hydrochloride (Tris-HCl) and DA were obtained from Shanghai Titan Co., Ltd., China. Mouse embryonic fibroblasts NIH/3T3 were acquired from the Cell Bank of the Chinese Academy of Sciences, and C57BL/6 mice were sourced from Shanghai Rise Biotechnology Co., Ltd., China. Poly-*L*-lactic acid (PLLA) was sourced from Nature Works, USA. Poly-*D*-lactic acid (PDLA) was acquired from Taiwan Plastics Industry Co., Ltd., China.

1.2 Synthesis of DMAPANO

DMAPANO was synthesized following previously established methods[23-25]. The synthesis route of DMAPANO is illustrated in Fig. 1. Specifically, in a 50 mL round-bottom flask, DMAPA (1.0 g) was dissolved in 10 mL deionized water. A total of 1.5 mL of a 30% H_2O_2 solution was added to the round-bottom flask. The flask was immersed in an oil bath maintained at 50 ℃, and the reaction was allowed to proceed for 6 h. Upon completion of the reaction, the resulting solution was dissolved in methanol, using a volume that was at least five times that of the reaction solution. Finally, the product was isolated by removing the solvent through vacuum distillation.

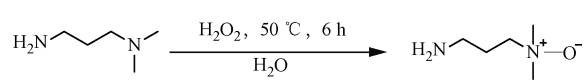


Fig. 1 Synthesis route of DMAPANO

1.3 Synthesis of PIA

According to the research conducted by Bednarz et al.[26], PIA was synthesized via the following procedure (Fig. 2), where n represents the number of IA units on the PIA chain. In a 250 mL round-bottom flask, IA (10.0 g) was dissolved in 50 mL of 0.5 mol/L HCl. The flask was then heated in an oil bath to 60 ℃, and APS (0.5 g) was added. The reaction was allowed to proceed for 36 h. Upon completion, the mixture was precipitated twice with acetone, yielding a white powder after vacuum drying. The product was subsequently re-dissolved in deionized water and subjected to dialysis for 4 d. The final product was obtained through freeze-drying.

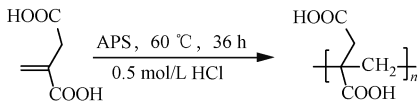


Fig. 2 Synthesis route of PIA

1.4 Synthesis of $PIANO_{50}$ and $PIANO_{70}$

PIA was dissolved in deionized water in separate 250 mL flasks for in-situ reaction. Subsequently, specific amounts of DMAPANO, corresponding to 50% and 70% of the molar ratio of —COOH, respectively, were added to the flasks. Following stirring at room temperature for 30 min, the respective DMTMM (equivalent to 100% DMAPA) was introduced into the flasks. After a 24 h reaction period, dialysis was conducted in deionized water for 4 d. The final product was obtained via freeze-drying. The synthesis route of $PIANO_{50}$ and $PIANO_{70}$ is shown in Fig. 3, where x and y denote the counts of IA units grafted with one and two TMAO zwitterionic monomers, respectively, with $x+y$ corresponding to the feeding molar ratio of TMAO to —COOH groups (50% or 70%).

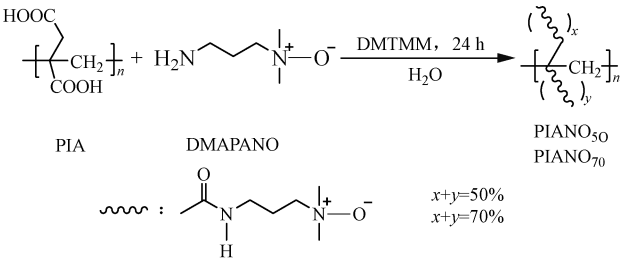


Fig. 3 Synthesis route of $PIANO_{50}$ and $PIANO_{70}$

1.5 Synthesis of $PIAPMANO_{50}$ and $PIAPMANO_{70}$

$PIANO_{50}$ or $PIANO_{70}$ was dissolved in deionized water in separate 250 mL round-bottom flasks, followed by the addition of varying amounts of APMA (equivalent to 30% and 50% of —COOH) dissolved beforehand in DMSO. After stirring the mixture for 30 min, distinct amounts of DMTMM (each equivalent to 100% of the respective APMA amount) were introduced. Following a 24 h reaction period, precipitation was induced by using a mixture of ethanol and ether (a volume ratio of 3∶1). Subsequently, the polymer was redissolved in deionized water, followed by a 4-day dialysis process. The resulting products, named $PIAPMANO_{50}$ and $PIAPMANO_{70}$, were obtained through freeze-drying. The synthesis route of $PIAPMANO_{50}$ and $PIAPMANO_{70}$ is shown in Fig. 4, where a and b represent the number of carboxyl-containing units in the —C═C— grafted PIA chain.

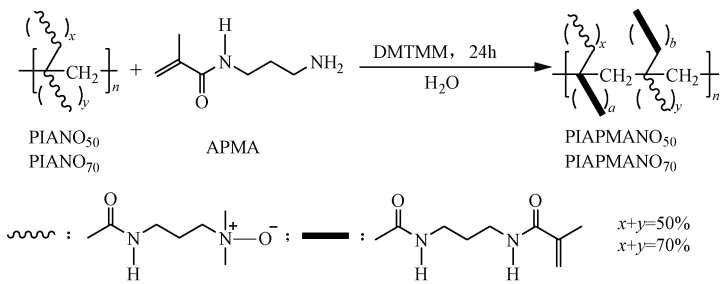


Fig. 4 Synthesis route of $PIAPMANO_{50}$ and $PIAPMANO_{70}$

1.6 Preparation of hydrogel precursor solutions

The hydrogel precursors $PIAPMANO_{50}$ or $PIAPMANO_{70}$ were dissolved in deionized water to achieve a mass fraction of 30%. The mixture was stirred thoroughly, followed by degassing the solution. Next, photoinitiator 1173 was incorporated at a mass fraction of 3% relative to the mass of the precursor. The solutions were stirred well and set aside.

1.7 Preparation of PLA electrospun nanofiber membranes

To enhance the mechanical properties of nanofiber membranes, equal masses of PLLA and PDLA were dissolved in a mixed solvent comprising HEIP and DMF at a mass fraction of 35%, with a volume ratio of HEIP to DMF of 5∶1. The solution was stirred thoroughly at room temperature to ensure complete dissolution of the polymers. Once a uniform and transparent solution was achieved, it was drawn into a syringe fitted with a flat needle tip of 0.86 mm inner diameter. The propulsion pump was set at a rate of 1 mL/h, with a high voltage of 8 kV and a distance of 10 cm between the needle and the collector. Electrospinning was conducted under controlled conditions at (25 ± 2) ℃ and a relative humidity of (65 ± 5)%. Following the completion of spinning, the nanofiber membrane was annealed at 70 ℃ for 12 h.

1.8 Preparation of PDA solution

DA was dissolved in a 0.1 mol/L Tris-HCl buffer solution, and then the pH was adjusted to 8.5 using NaOH to induce the oxidative self-polymerization of DA, yielding the PDA solution.

1.9 Preparation of PLA@PDA@PIAPMANO$_{50}$ and PLA@PDA@PIAPMANO$_{70}$

PLA was soaked in the aforementioned DA solution for 12 h to facilitate the self-polymerization of DA on the PLA surface, resulting in a PDA coating. Following the soaking period, the PLA was rinsed with deionized water to eliminate any PDA particles that were adhered to its surface. Subsequently, the treated PLA was immersed in the hydrogel precursor solution for 30 min. After this immersion, the PLA was removed and exposed to a 365 nm wavelength UV lamp for 1 h to induce the polymerization of the hydrogel precursor, thereby forming a hydrogel coating on the PLA surface. Consequently, hydrogel-nanofiber membranes with multilayer structures were created and designated as PLA@PDA@PIAPMANO$_{50}$ and PLA@PDA@PIAPMANO$_{70}$, respectively.

1.10 Test and characterization

1.10.1 Chemical structure and physical property

The chemical structures of PLA, PLA@PDA, and PLA@PDA@PIAPMANO were analyzed by a Fourier transform infrared (FTIR) spectrometer (Spectrum II, PerkinElmer, USA). Rectangular specimens of 75 mm × 5 mm were prepared, and tensile property tests were conducted by using a universal material testing machine (H10K-S, Tinius Olsen, USA). The water contact angle (WCA) test was carried out by using a contact angle measuring instrument (DSA30, KRUSS, Germany). The surface morphology of the sample was observed by using a field emission scanning electron microscope (S-4800, Hitachi, Japan). The cubic samples (10 mm × 10 mm × 2 mm) were immersed in deionized water at room temperature for swelling performance testing. The swelling rate R_s was calculated as

$$R_s = \frac{m_s - m_0}{m_0}, \tag{1}$$

where m_0 denotes the mass of the prepared composite; m_s indicates the mass of the composite following swelling. The experiment was performed three times, and the recorded values represent the average.

1.10.2 Protein adsorption

The samples were immersed in 0.02 mg/mL FITC-BSA solution and incubated in the dark for 4 h. Afterward, the FITC-BSA solution was discarded, and the samples were rinsed with PBS buffer. The surface fluorescence intensity of the samples was measured by using an inverted fluorescence microscope (DMiL, Leica, Germany).

1.10.3 Cell adhesion assay

After co-culturing the samples with NIH/3T3 cells at a density of 2×10^5 cells mL^{-1} for 24 h, the culture medium was removed. The cells were stained with Calcein/PI cell viability and cytotoxicity assay reagents, and the cell adhesion was observed by using the inverted fluorescence microscope.

1.10.4 Cytotoxicity

The samples were co-cultured with 1×10^4 NIH/3T3 cells for 24, 48, and 72 h. Afterward, the CCK-8 reagent was added. The absorbance at 450 nm was measured by a microplate reader to quantitatively evaluate the cell viability. The cell viability C was calculated as

$$C = \frac{A_t - A_0}{A_c - A_0} \times 100\%, \tag{2}$$

where A_t denotes the absorbance of the experimental group; A_0 represents the absorbance of the DMEM medium; A_c signifies the absorbance of the control group.

1.10.5 In vivo biocompatibility

Sterilized samples were implanted into the abdominal cavity of C57BL/6J mice. The mice were divided into two groups and kept for 14 d and 30 d, respectively. Afterward, all mice were euthanized, and the hydrogel samples, together with the surrounding tissues, were carefully dissected and collected. The tissue sections were stained with Hematoxylin-Eosin (H & E) and Masson trichrome. The stained sections were observed in detail and photographed under an optical microscope. Collagen density was assessed by quantifying the blue coverage of tissues within a 50 μm range at intervals of 10 μm from the hydrogel-tissue interface in Masson trichrome-stained images. The collagen density and capsule thickness were analyzed by using ImageJ software based on the Masson trichrome-stained images[27]. All experimental animal procedures were conducted in strict accordance with animal welfare laws and guidelines and were approved by the Animal Ethics Committee of Donghua University, China (DWSY202503160140).

1.10.6 Statistical analysis

The bar charts and dot plots presented in this study illustrated the mean and standard deviation of the data. Statistical analysis was performed by Student's t-test, with a p value of less than 0.05 deemed statistically significant.

2 Results and Discussion

2.1 Structural characterization of PLA@PDA and PLA@PDA@PIAPMANO$_{50}$

PLA nanofiber membranes were initially immersed in a PDA solution. Following continuous treatment at room temperature for 12 h, the originally white PLA exhibited a gray coloration. This color change serves as an initial indication that PDA has been deposited on the surface of PLA. To confirm the deposition of PDA and PIAPMANO$_{50}$ on the surface of PLA, FTIR was employed for analysis. The results are illustrated in Fig. 5. The spectrum of unprocessed PLA exhibits in-

plane bending vibration peaks of O—H at 1 450 cm^{-1}. Additionally, the C—H stretching vibration peaks and in-plane bending vibration peaks associated with alkanes are observed at 2 990, 2 940, and 1 380 cm^{-1}. The peaks at 1 750 and 1 265 cm^{-1} correspond to the C═O stretching vibration and the C—O—C stretching vibration of the ester group, while the peaks at 1 300 cm^{-1} indicate the C—O stretching vibration of the carboxylic acid. The spectra of PLA@PDA and PLA@PDA@$PIAPMANO_{50}$ retain these characteristic peaks. Furthermore, three new peaks at 3 330, 1 610, and 1 510 cm^{-1} emerge, corresponding to the N—H stretching vibration, N—H bending vibration, and aromatic ring stretching vibration of the primary amine in PDA, respectively[28-30].

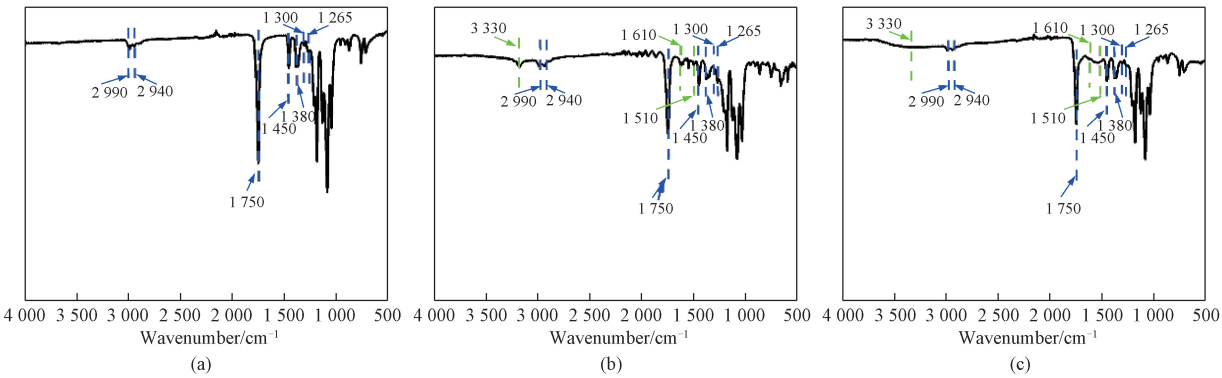


Fig. 5 FTIR spectra of different materials: (a) PLA; (b) PLA@PDA; (c) PLA@PDA@$PIAPMANO_{50}$

2.2 Physical properties of PLA@PDA@$PIAPMANO_{50}$ and PLA@PDA@$PIAPMANO_{70}$

2.2.1 Microscopic characteristic

To examine the surface microscopic characteristics of PLA@PDA@$PIAPMANO_{50}$ and PLA@PDA@$PIAPMANO_{70}$ composites during the preparation process, scanning electron microscopy (SEM) was employed. The results presented in Fig. 6 reveal several notable features. First, the fiber structure of PLA is uniform and dense, with a diameter of approximately 0.7 μm. This consistent fiber architecture establishes a solid foundation for subsequent coating treatments. Subsequent treatment of PLA with DA solution results in notable alterations to the fiber surface. The SEM image illustrates the successful formation of a PDA layer that covers the surface of the PLA fibers. This modification not only improves the surface properties of PLA but also offers adhesion points for the subsequent hydrogel coating. PLA@PDA composites were immersed in hydrogel precursor solutions containing $PIAPMANO_{50}$ and $PIAPMANO_{70}$, respectively. Following the treatment under light conditions, a thick hydrogel layer formed on the fiber surface.

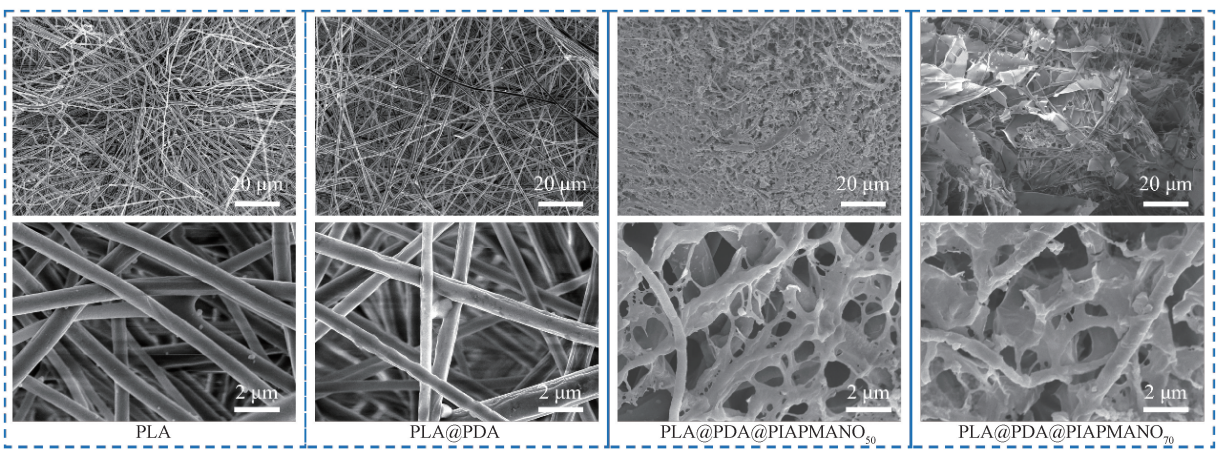


Fig. 6 SEM images of different materials: (a) PLA; (b) PLA@PDA; (c) PLA@PDA@$PIAPMANO_{50}$; (d) PLA@PDA@$PIAPMANO_{70}$

2.2.2 Swelling behavior

To address the potential instability of implant structures resulting from the swelling behavior of hydrogels[31], the present study characterized the swelling behavior of PLA@PDA@$PIAPMANO_{50}$ and PLA@PDA@$PIAPMANO_{70}$ composites using a swelling kinetics testing system. A comparative analysis was conducted with the pure $PIAPMANO_{50}$ and $PIAPMANO_{70}$ hydrogels. This analysis aimed to evaluate the regulatory effect of the composite structure on the swelling behavior. The experimental results are presented in Fig. 7. For both the pure hydrogels and the PLA-based composites, the

swelling ratio increases as the zwitterion dosage increases. This result is mainly attributed to the fact that an increase in the zwitterion dosage leads to a corresponding decrease in the amount of cross-linkable carbon-carbon double bonds. This consequently reduces the cross-linking density of the pure hydrogels or the composites, as well as the resistance to water molecule penetration into the hydrogel matrix. Therefore, the sample with a 70% zwitterion dosage exhibits a significantly higher swelling ratio than that with a 50% zwitterion dosage. The swelling ratios of the composites are significantly lower than those of the control group hydrogels. This swelling inhibition arises from two primary mechanisms. First, PLA nanofibers, which serve as the base material of the composite, exhibit extremely low inherent swelling properties, thereby physically restricting the volume expansion of the composite. Second, the surface-modified PDA coating further restricts the swelling potential by enhancing interfacial adhesion. This synergistic dual effect allows the composite to maintain structural stability while effectively mitigating the risk of the implant shape deformation due to excessive swelling in traditional hydrogels.

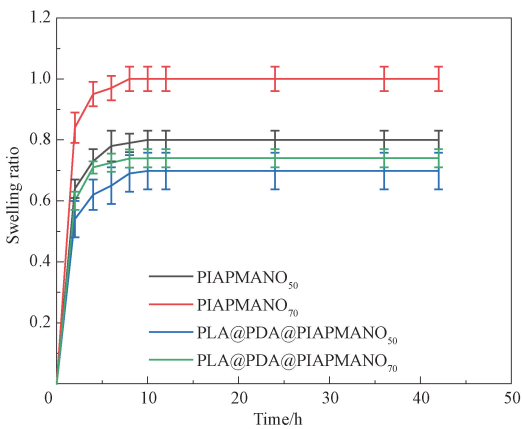
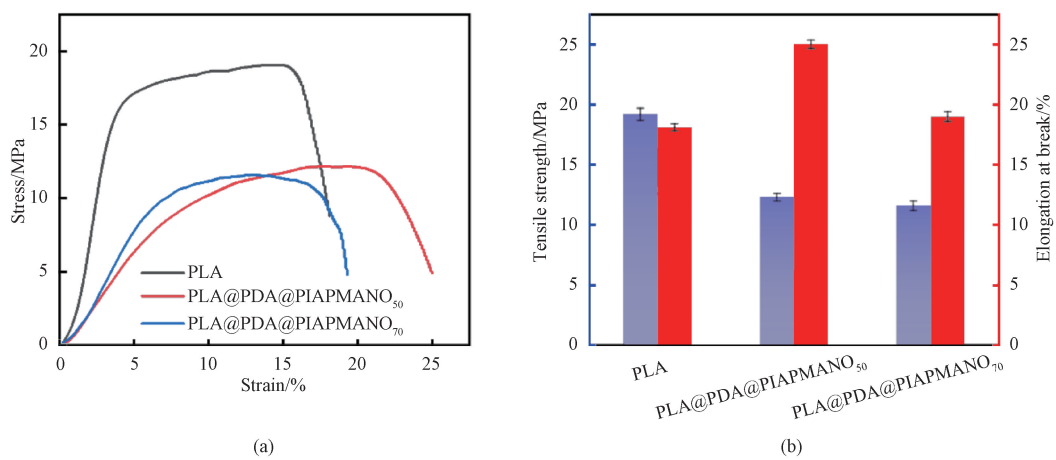


Fig. 7 Swelling ratio of $PIAPMANO_{50}$, $PIAPMANO_{70}$, PLA@PDA@$PIAPMANO_{50}$, and PLA@PDA@$PIAPMANO_{70}$

2.2.3 Mechanical properties

The mechanical properties of PLA, PLA@PDA@$PIAPMANO_{50}$, and PLA@PDA@$PIAPMANO_{70}$ composites were characterized by using a universal material testing machine. The results are presented in Fig. 8. The tensile strength of pure PLA is 19 MPa, and the elongation at break is 18%. Following the deposition of the PDA coating onto the PLA surface, a reduction in the tensile strength of the composite is noted, accompanied by an increase in the elongation at break. PLA@PDA@$PIAPMANO_{50}$ shows a tensile strength of approximately 13 MPa and an elongation at break exceeding 20%. The occurrence of this phenomenon can be attributed to several factors. First, the hydrogel deposited on the surface of PLA forms a cross-linked network structure with a high water content. In comparison to PLA, the mechanical strength of this hydrogel network is relatively low. Consequently, when the composite is stretched, the hydrogel layer becomes a weak link due to its diminished tensile strength, resulting in a decrease in overall tensile strength. Second, the flexible cross-linked network of the hydrogel exhibits extensive reversible deformation capabilities during the stretching process. This characteristic allows the composites to better absorb and disperse stresses when subjected to external forces, thereby enhancing the ductility. Although the tensile strength has diminished, the increase in the elongation at break suggests that the composites, while retaining a certain level of strength, exhibit enhanced flexibility and ductility. Notably, the composites show marked superiority in mechanical properties compared to the pure hydrogels. Pure hydrogels possess extremely poor mechanical properties, characterized by brittleness and fragility, which preclude their use in tensile tests. Compared to the pure hydrogels, the composites formed by combining PLA nanofibers with the hydrogels exhibit significantly enhanced mechanical properties, maintaining a certain strength while offering good flexibility.



(a) (b)

Fig. 8 Mechanical properties of PLA, PLA@PDA@$PIAPMANO_{50}$ and PLA@PDA@$PIAPMANO_{70}$: (a) stress-strain curves; (b) tensile strength and elongation at break

2.3 In vitro antifouling property

2.3.1 Hydrophilic property

The hydrophilicity of a material's surface is critical in preventing the adhesion of cells and proteins. Hydrophilic surfaces exhibit strong interactions with water molecules, leading to the formation of a dense and stable hydration layer. This hydration layer serves as a physical barrier that significantly impedes the non-specific adsorption of proteins. The WCA measurement was employed to assess the hydrophilicity of the surface of the PLA@PDA@PIAPMANO$_{50}$ and PLA@PDA@PIAPMANO$_{70}$ composites. The test results presented in Fig. 9 indicate that the surface of the pure PLA membrane displays a hydrophobic characteristic, with a WCA exceeding 90°. In contrast, the deposition of PDA on the PLA membrane surface results in a significant reduction in the WCA, thereby rendering the surface of the PLA@PDA hydrophilic. This transformation is attributed to the abundance of polar groups, including phenolic hydroxyl groups and amino groups, in PDA molecules. These polar groups facilitate strong interactions with water molecules, thereby markedly increasing the hydrophilicity of the material surface[32]. Following the formation of the PIAPMANO$_{50}$ and PIAPMANO$_{70}$ hydrogel layers on the PLA substrate, the hydrophilicity of the composite's surface exhibits a marked improvement compared to both the pure PLA nanofiber membrane and the nanofiber membrane treated with PDA. This enhancement is primarily attributed to the TMAO zwitterionic structure present in the PIAPMANO$_{50}$ and PIAPMANO$_{70}$ hydrogel layers. The TMAO zwitterionic structure, characterized by its short dipole moment, engages in strong electrostatic interaction with water molecules. Consequently, this interaction facilitates the formation of a dense and stable hydration layer on the surface of the composite, thereby significantly augmenting its hydrophilicity.

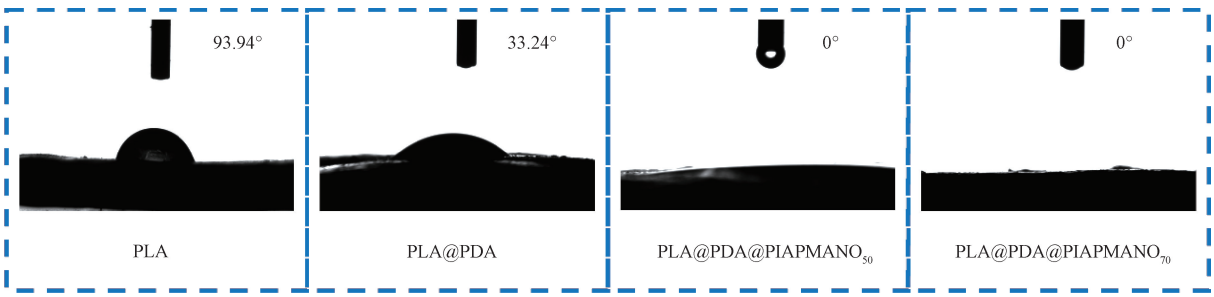


Fig. 9 WCAs of different materials: (a) PLA; (b) PLA@PDA; (c) PLA@PDA@PIAMANO$_{50}$; (d) PLA@PDA@PIAMANO$_{70}$

2.3.2 Anti-adhesion to protein and cells

Numerous studies have demonstrated that non-specific protein adsorption on implant surfaces is a critical initial step in the development of the foreign body reaction. Accordingly, FITC-BSA was employed as a model protein to assess the adsorption characteristics of PLA@PDA@PIAPMANO$_{50}$ and PLA@PDA@PIAPMANO$_{70}$ composites. The test results presented in Fig. 10 indicate that a substantial amount of protein adheres to the surface of both pure PLA nanofiber membrane and PEG hydrogel. The protein adsorption rate on the PEG hydrogel surface is slightly lower than that on PLA. This difference arises because the PEG hydrogel surface is rich in —OH groups, which can form a hydration layer through hydrogen bonding, thereby impeding protein adsorption. In contrast, protein adsorption on the surfaces of PLA@PDA@PIAPMANO$_{50}$ and PLA@PDA@PIAPMANO$_{70}$ is significantly reduced to less than 30% relative to that of PLA, which is set at 100%. These results indicate that the PIAPMANO$_{50}$ and PIAPMANO$_{70}$ hydrogels can create a hydrated layer on the surface of PLA, thereby improving the antifouling performance of the composite. Furthermore, the protein adsorption rate of this composite is significantly superior to that of PEG hydrogel, which can be attributed to the presence of the TMAO structure on the composite's surface. In contrast to the —OH groups found on the surface of PEG hydrogel, TMAO facilitates electrostatic interactions with water molecules, resulting in a denser hydrated layer and enhanced anti-protein adsorption capabilities. Additionally, as the amount of the zwitterionic component increases, the protein adsorption capacity markedly decreases. This observation further substantiates the critical role of the TMAO structure in augmenting the antifouling performance of composite materials.

To further investigate the in vitro antifouling properties of PLA@PDA@PIAPMANO$_{50}$ and PLA@PDA@PIAPMANO$_{70}$ composites, we conducted cell adhesion experiments using mouse embryonic fibroblasts (NIH/3T3 cells). The experimental results, presented in Fig. 11, are highly consistent with the aforementioned findings regarding protein adhesion. Specifically, NIH/3T3 cells adhered to the surfaces of pure PLA nanofiber membranes and PEG hydrogel in substantial quantities. In contrast, the number of adherent cells on the surfaces of PLA@PDA@PIAPMANO$_{50}$ and PLA@PDA@PIAPMANO$_{70}$ composites is nearly negligible. This finding suggests that the PIAPMANO$_{50}$ and PIAPMANO$_{70}$ hydrogel layers significantly enhance the antifouling performance of the composite.

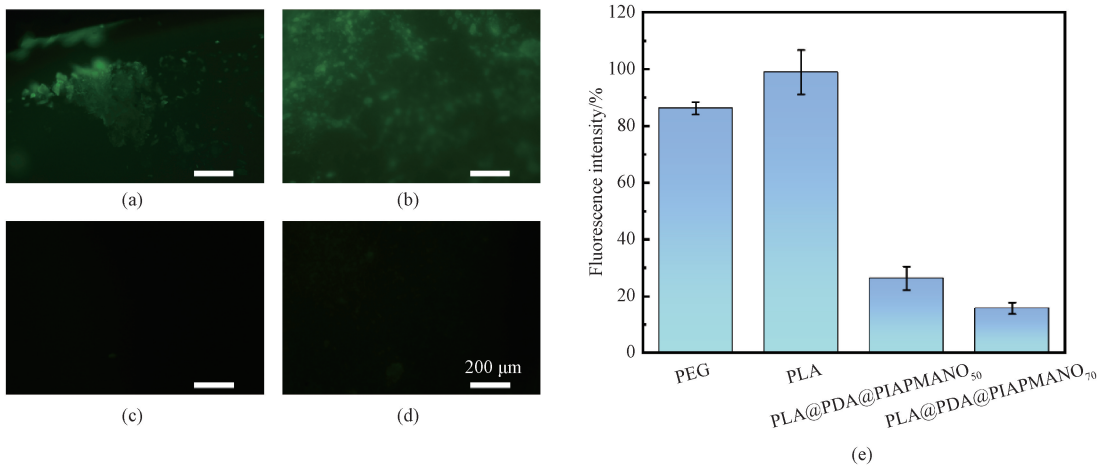


Fig. 10 Protein adhesion and fluorescence intensity of different materials: (a) PEG; (b) PLA; (c) PLA@PDA@PIAPMANO$_{50}$; (d) PLA@PDA@PIAPMANO$_{70}$; (e) fluorescence intensity

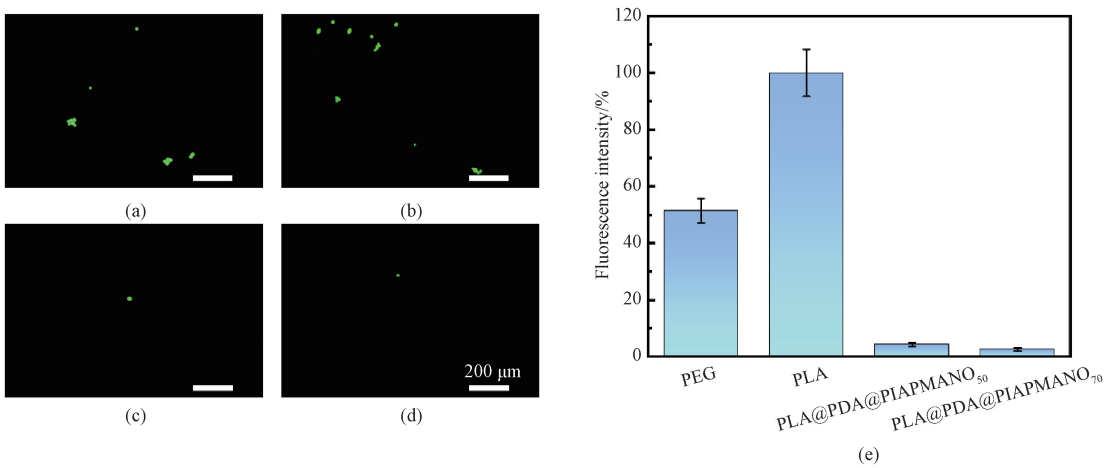


Fig. 11 Cell adhesion and fluorescence intensity of different materials: (a) PEG; (b) PLA; (c) PLA@PDA@PIAPMANO$_{50}$; (d) PLA@PDA@PIAPMANO$_{70}$; (e) fluorescence intensity

2.4 Cytotoxicity and in vivo compatibility

For an implant material, the core requirements include not only the reduction of the foreign body reaction but also the assurance of material safety and non-toxicity to cells. Consequently, before the implantation of PLA@PDA@PIAPMANO$_{50}$ and PLA@PDA@PIAPMANO$_{70}$ composites into mice, it is essential to evaluate their cytotoxicity. The experimental results are presented in Fig. 12. The PEG hydrogel, pure PLA nanofiber membrane, PLA@PDA@PIAPMANO$_{50}$, and PLA@PDA@PIAPMANO$_{70}$ composites demonstrate cell activity comparable to that of the control group. This finding indicates that these materials do not adversely affect the cell activity. Over time, the cell viability continues to rise, reflecting a favorable growth state. In conclusion, these materials exhibit low cytotoxicity, highlighting their significant potential for in vivo applications.

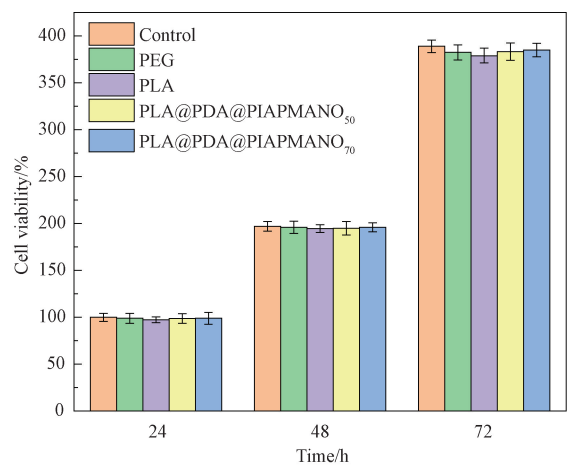
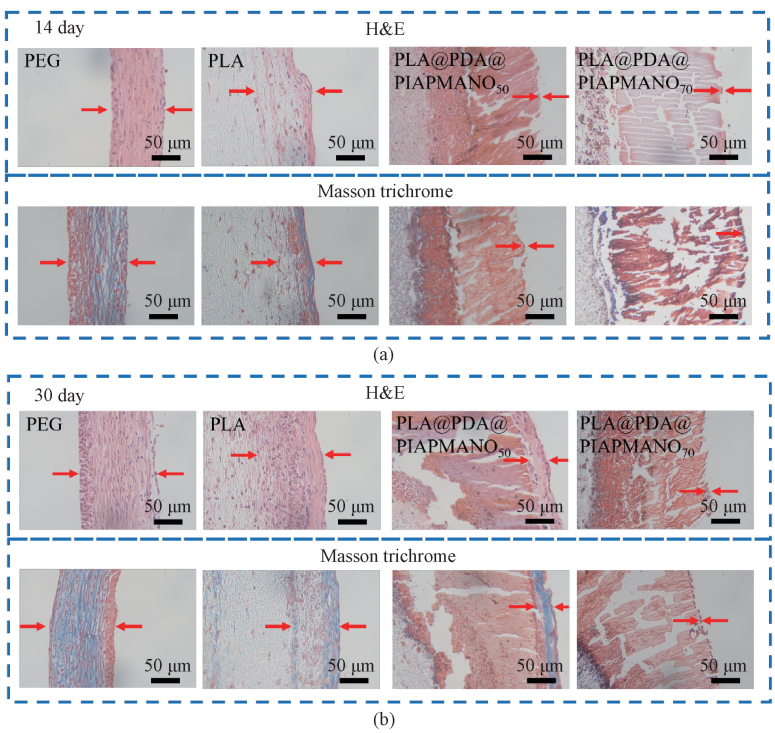


Fig. 12 Effects of PEG, PLA, PLA@PDA@PIAPMANO$_{50}$, and PLA@PDA@PIAPMANO$_{70}$ on cell viability

Building on the impressive performance of PLA@PDA@PIAPMANO$_{50}$ and PLA@PDA@PIAPMANO$_{70}$ composites in cytotoxicity and in vitro antifouling tests, we further assessed their in vivo anti-foreign body reaction through intraperitoneal implantation in C57BL/6 mice. Established patterns of host response to biomaterial implantation indicate that acute inflammation typically arises within one week, while collagen capsule formation associated with chronic inflammation often manifests after three weeks. Following these patterns, systematic analyses were conducted on the 14th day (acute/subacute phase) and the 30th day (chronic phase) post-implantation. At each time point, the material was removed, and the inflammatory cells adhered to its surface were examined by using H&E staining. H&E staining reagents can color tissue cell nuclei blue or purple, while collagen and muscle appear red. Concurrently, the fibrosis surrounding the implant was assessed through Masson trichrome staining. Masson trichrome staining reagents can color collagen blue or purple, cytoplasm red, and cell nuclei black[33]. At the 14th day post-implantation, both H&E and Masson trichrome staining reveal that immune cells have aggregated on the surfaces of all materials (Fig. 13 (a)), confirming that the implants elicit the host's innate immune response. The inflammatory cell adhesion levels of the PLA@PDA@PIAPMANO$_{50}$ and PLA@PDA@PIAPMANO$_{70}$ composites are significantly lower than those observed in pure PLA nanofiber membranes and PEG hydrogel. Quantitative analysis using Masson trichrome staining (Fig. 13 (c)) indicates that the collagen deposition thickness in the control groups (PLA and PEG) surpasses 120 μm, whereas that in the composite groups is below 10 μm, demonstrating a statistically significant difference ($p < 0.05$). The data at this stage indicate that PIAPMANO$_{50}$ and PIAPMANO$_{70}$ hydrogels have established an effective antifouling layer on the surface of the PLA nanofiber membrane, which significantly inhibits the interfacial aggregation of early inflammatory cells. During the chronic phase assessment conducted 30 days post-implantation, a dense and avascular collagen layer (thickness >120 μm) developed at the interface between the material and the tissue in the control group, exhibiting characteristics typical of a foreign body reaction (Fig. 13(d)). In contrast, the interface of the composite group displays only sparse and discontinuous collagen deposits, with an average thickness of less than 30 μm (Fig. 13 (d)). This notable inhibitory effect on fibrosis can be attributed to two factors. First, the sustained anti-protein adsorption property of the PIAPMANO$_{50}$ and PIAPMANO$_{70}$ hydrogels obstructs the fibroblast activation signal. Second, the PDA intermediate layer enhances the interface stability and prevents the hydrogel layer from detaching. The results from the acute and chronic two-stage experiments indicate that the PLA@PDA@PIAPMANO$_{50}$ and PLA@PDA@PIAPMANO$_{70}$ composites exhibit exceptional in vivo performance against the foreign body reaction. This is achieved through the establishment of a multi-level defense system, which includes surface and interface antifouling layers that inhibit acute inflammation, as well as a three-dimensional structural regulation that delays the fibrosis process.



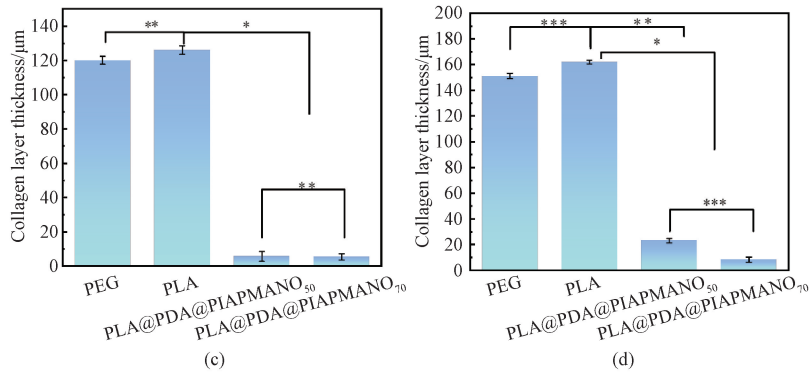


Fig. 13 In vivo anti-foreign body reaction efficacy of different materials: (a) H&E and Masson trichrome staining of sample implanted in vivo for 14 d; (b) H&E and Masson trichrome staining of sample implanted in vivo for 30 d; (c) collagen layer thickness on surface of sample implanted in vivo for 14 d; (d) collagen layer thickness on surface of sample implanted in vivo for 30 d

3 Conclusions

In conclusion, we have successfully synthesized a nanofiber/zwitterionic hydrogel composite that integrates the distinct advantages of both hydrogels and nanofibers. This composite exhibits the remarkable flexibility and stretchability of nanofibers, which enhance the mechanical properties and mitigate the fragility inherent in hydrogels. Additionally, the hydrogel layer on the surface of the composite substantially increases the hydrophilicity of the nanofiber membrane, thereby imparting exceptional resistance to biological contamination. Upon implantation into the abdominal cavity of mice, the presence of the TMAO zwitterionic structure facilitates the formation of a dense and stable hydrated layer on the composite's surface. Consequently, in comparison to the PEG hydrogel and PLA nanofiber membrane, this composite significantly decreases the adsorption rate of inflammatory cells on the implant surface and reduces the thickness of the collagen layer, demonstrating a pronounced anti-foreign body reaction.

References

[1] Song Y, Li L H, Zhao W K, et al. Surface modification of electrospun fibers with mechano-growth factor for mitigating the foreign-body reaction[J]. *Bioactive Materials*, 2021, 6(9): 2983-2998.

[2] Zhang D H, Chen Q, Shi C, et al. Dealing with the foreign-body response to implanted biomaterials: strategies and applications of new materials[J]. *Advanced Functional Materials*, 2021, 31(6): 2007226.

[3] Franz S, Rammelt S, Scharnweber D, et al. Immune responses to implants: a review of the implications for the design of immunomodulatory biomaterials[J]. *Biomaterials*, 2011, 32(28): 6692-6709.

[4] Kondyurina I, Kondyurin A. Foreign body reaction (immune response) for artificial implants can be avoided: an example of polyurethane in mice for 1 week[J]. *Journal of Functional Biomaterials*, 2023, 14(8): 432.

[5] Puskas J E, Luebbers M T. Breast implants: the good, the bad and the ugly. Can nanotechnology improve implants [J]. *Wiley Interdisciplinary Reviews Nanomedicine and Nanobiotechnology*, 2012, 4(2): 153-168.

[6] Zhou X C, Wang Y X, Ji J, et al. Materials strategies to overcome the foreign body response [J]. *Advanced Healthcare Materials*, 2024, 13 (18): 2304478.

[7] Dong Y P, Zheng Y Q, Zhang K Y, et al. Electrospun nanofibrous materials for wound healing[J]. *Advanced Fiber Materials*, 2020, 2 (4): 212-227.

[8] Huang W, Xiao Y C, Shi X Y. Construction of electrospun organic/inorganic hybrid nanofibers for drug delivery and tissue engineering applications [J]. *Advanced Fiber Materials*, 2019, 1(1): 32-45.

[9] Sill T J, Von Recum H A. Electrospinning: applications in drug delivery and tissue engineering[J]. *Biomaterials*, 2008, 29(13): 1989-2006.

[10] Woo K M, Chen V J, Ma P X. Nano-fibrous scaffolding architecture selectively enhances protein adsorption contributing to cell attachment [J]. *Journal of Biomedical Materials Research Part A*, 2003, 67A(2): 531-537.

[11] Lucke S, Walschus U, Hoene A, et al. The in vivo inflammatory and foreign body giant cell response against different poly(*L*-lactide-*co*-*D*/*L*-lactide) implants is primarily determined by material morphology rather than surface chemistry [J]. *Journal of Biomedical Materials Research Part A*, 2018, 106(10): 2726-2734.

[12] Grafahrend D, Heffels K H, Beer M V, et al. Degradable polyester scaffolds with controlled

surface chemistry combining minimal protein adsorption with specific bioactivation[J]. *Nature Materials*, 2011, 10(1): 67-73.
[13] Cheng L, Wang Y, Sun G M, et al. Hydration-enhanced lubricating electrospun nanofibrous membranes prevent tissue adhesion [J]. *Research*, 2020, 2020: 4907185.
[14] Yang W J, Sundaram H S, Ella J R, et al. Low-fouling electrospun PLLA films modified with zwitterionic poly (sulfobetaine methacrylate)-catechol conjugates [J]. *Acta Biomaterialia*, 2016, 40: 92-99.
[15] Ratner B D. Reducing capsular thickness and enhancing angiogenesis around implant drug release systems [J]. *Journal of Controlled Release*, 2002, 78(1/2/3): 211-218.
[16] Lynn A D, Kyriakides T R, Bryant S J. Characterization of the in vitro macrophage response and in vivo host response to poly (ethylene glycol)-based hydrogels[J]. *Journal of Biomedical Materials Research Part A*, 2010, 93A(3): 941-953.
[17] Chen S F, Li L Y, Zhao C, et al. Surface hydration: principles and applications toward low-fouling/nonfouling biomaterials [J]. *Polymer*, 2010, 51(23): 5283-5293.
[18] Zhang L, Cao Z Q, Bai T, et al. Zwitterionic hydrogels implanted in mice resist the foreign-body reaction[J]. *Nature Biotechnology*, 2013, 31(6): 553-556.
[19] Cao B, Tang Q, Li L L, et al. Switchable antimicrobial and antifouling hydrogels with enhanced mechanical properties [J]. *Advanced Healthcare Materials*, 2013, 2(8): 1096-1102.
[20] Zhang M M, Xu S X, Wang R Y, et al. Electrospun nanofiber/hydrogel composite materials and their tissue engineering applications [J]. *Journal of Materials Science & Technology*, 2023, 162: 157-178.
[21] Gelain F, Luo Z L, Zhang S G. Self-assembling peptide EAK16 and RADA16 nanofiber scaffold hydrogel [J]. *Chemical Reviews*, 2020, 120 (24): 13434-13460.
[22] Islam M A, Wang R J, Chen W, et al. Flax/polylactic acid (PLA) core/sheath structural composite yarn fabricated by spindle braiding technique[J]. *Journal of Donghua University (English Edition)*, 2024, 41(5): 451-460.
[23] Zhang N, Cheng K, Zhang J J, et al. A dual-biomimetic strategy to construct zwitterionic anti-fouling membrane with superior emulsion separation performance [J]. *Journal of Membrane Science*, 2022, 660: 120829.
[24] Zhou Z, Shi Q H. Bioinspired dopamine and *N*-oxide-based zwitterionic polymer brushes for fouling resistance surfaces[J]. *Polymers*, 2024, 16(12):1634.
[25] Kumar R, Mancebo J G, Patenaude R, et al. Low-fouling zwitterionic polymeric colloids as resuscitation fluids for hemorrhagic shock [J]. *Advanced Materials*, 2022, 34(47): 2207376.
[26] Bednarz S, Wesołowska-Piętak A, Konefał R, et al. Persulfate initiated free-radical polymerization of itaconic acid: kinetics, end-groups and side products[J]. *European Polymer Journal*, 2018, 106: 63-71.
[27] Zhou X C, Cao W Z, Chen Y C, et al. An elastomer with in situ generated pure zwitterionic surfaces for fibrosis-resistant implants[J]. *Acta Biomaterialia*, 2024, 185: 226-239.
[28] Dai S Y, Yue S S, Ning Z B, et al. Polydopamine nanoparticle-reinforced near-infrared light-triggered shape memory polycaprolactone-polydopamine polyurethane for biomedical implant applications[J]. *ACS Applied Materials & Interfaces*, 2022, 14(12): 14668-14676.
[29] Ma F F, Zhang N, Wei X, et al. Blend-electrospun poly (vinylidene fluoride)/polydopamine membranes: self-polymerization of dopamine and the excellent adsorption/separation abilities[J]. *Journal of Materials Chemistry A*, 2017, 5(27): 14430-14443.
[30] Zhou M, Liu Q, Wu S S, et al. Starch/chitosan films reinforced with polydopamine modified MMT: effects of dopamine concentration [J]. *Food Hydrocolloids*, 2016, 61: 678-684.
[31] Zhan Y W, Fu W J, Xing Y C, et al. Advances in versatile anti-swelling polymer hydrogels[J]. *Materials Science and Engineering: C*, 2021, 127:112208.
[32] Fu Y, Yang L, Zhang J H, et al. Polydopamine antibacterial materials[J]. *Materials Horizons*, 2021, 8(6):1618-1633.
[33] Wang X, Maxwell K G, Wang K, et al. A nanofibrous encapsulation device for safe delivery of insulin-producing cells to treat type 1 diabetes [J]. *Science Translational Medicine*, 2021, 13 (596): eabb4601.

纳米纤维/两性离子水凝胶复合材料用于抗异物反应

党向宇，高玉洁，陈支泽*
东华大学 绿色低碳纺织印染技术教育部重点实验室，化学与化工学院，上海 201620

摘　要：在本研究中，我们制备了一种纳米纤维/两性离子水凝胶复合材料，用于体内抗异物反应。该复合材料利用聚多巴胺的黏合作用，将三甲胺 *N*-氧化物两性离子水凝胶与立构复合聚乳酸纳米纤维膜结合在一起。所得复合材料具有聚乳酸良好的力学性能，拉伸强度为 13 MPa 左右，断裂伸长率超过 20%。同时，由于三甲胺 *N*-氧化物两性离子水凝胶的作用，该复合材料表现出优异的抗生物污染性能。复合材料植入在小鼠体内 30 天后，表面仍未形成致密的胶原层，其厚度维持在 30 μm 以内。

关键词：纳米纤维；水凝胶；抗异物反应；两性离子